The Mass Ratio Distribution of Black Hole Mergers Induced by a Comparable Mass Tertiary

Accepted XXX. Received YYY; in original form ZZZ

ABSTRACT

Abstract

Key words: binaries:close – stars:black holes

1 INTRODUCTION

We study the von Zeipel-Lidov-Kozai effect (ZLK) for eccentric perturbers to octupole order, also sometimes known as the eccentric Kozai mechanism (e.g. Lithwick & Naoz 2011).

The mass ratio distribution among ZLK-induced BBH mergers has already been noted (see Fig. 10 of Silsbee & Tremaine 2017), but the origin of the effect has not been carefully studied.

2 DYNAMICS WITHOUT GRAVITATIONAL WAVE RADIATION

We first briefly review results in regimes of increasing complexity.

We use the octupole-order, double-averaged vectorial ZLK equations from LML15 (Liu et al. 2015), including 1PN de Sitter apsidal precession. In this section, we neglect 2.5PN GW radiation (Peters 1964), but will consider it later in Section 3.

2.1 Quadrupole-Order ZLK

When considering the EOM to quadrupole order, the eccentricity of the inner binary cycles regularly over $\sim t_{\rm ZLK}$ with

$$t_{\rm LK} = \frac{1}{n_1}\frac{m_{12}}{m_3}\left(\frac{a_{\rm out,eff}}{a}\right)^3, \tag{1}$$

where $a_{\rm out,eff} \equiv a_{\rm out}\sqrt{1-e_{\rm out}^2}$. Our fiducial parameters are: $a = 100$ AU, $a_{\rm out,eff} = 3600$ AU, $m_{12} = 50M_\odot$, $m_3 = 30M_\odot$.

The dynamics to quadrupole order depend on the ratio of the angular momenta, given by

$$\eta \equiv \left.\frac{L}{L_{\rm out}}\right|_{e=0} = \frac{\mu}{\mu_{\rm out}}\left[\frac{m_{12}a}{m_{123}a_{\rm out}\left(1-e_{\rm out}^2\right)}\right]^{1/2}. \tag{2}$$

Note that to quadrupolar order, $e_{\rm out}$ and thus η are constant.

We further have the following results:

- The system spends a fraction $\sim j(e_{\rm max})$ of each ZLK eccentricity cycle near $e_{\rm max}$ (Anderson et al. 2016).
- Two conserved quantities, energy and $K \equiv j\cos I - \eta e^2/2$. K is the general conserved quantity which when $\eta = 0$ reduces to the classical "Kozai Constant" (Liu et al. 2015).

When 1PN is considered, the strength is measured by

$$\epsilon_{\rm GR} \equiv \frac{3Gm_{12}}{c^2}\frac{m_{12}}{m_3}\frac{a_{\rm out,eff}^3}{a^4}. \tag{3}$$

This gives further results:

- It can be shown that $e_{\rm max}$ and $j_{\rm min} \equiv j(e_{\rm max})$ for a given I_0 obeys (Liu et al. 2015; Anderson et al. 2016):

$$\frac{3}{8}\frac{j_{\rm min}^2-1}{j_{\rm min}^2}\left[5\left(\cos I_0+\frac{\eta}{2}\right)^2-\left(3+4\eta\cos I_0+\frac{9}{4}\eta^2\right)j_{\rm min}^2 + \eta^2 j_{\rm min}^4\right]+\epsilon_{\rm GR}\left(1-1/j_{\rm min}\right)=0. \tag{4}$$

The minimum value of $j_{\rm min}$, denoted $j_{\rm lim}$, occurs when $I_0 = I_{0,\rm lim}$, where

$$\cos I_{0,\rm lim} = \frac{\eta}{2}\left(\frac{4}{5}j_{\rm lim}^2-1\right). \tag{5}$$

Note that $I_{0,\rm lim} \geq 90^\circ$ with equality only when $\eta = 0$. Substituting Eq. (5) into Eq. (4) gives

$$\frac{3}{8}\left(j_{\rm lim}^2-1\right)\left[-3+\frac{\eta^2}{4}\left(\frac{4}{5}j_{\rm lim}^2-1\right)\right]+\epsilon_{\rm GR}\left(1-1/j_{\rm lim}\right)=0. \tag{6}$$

2.2 Octupole-Order ZLK, Test-Particle Limit

Well-studied in test particle limit where $m_2 = 0$ and $\eta = 0$, we review a few relevant results. In this limit, define

$$\epsilon_{\rm oct}^{\rm (tp)} = \frac{a}{a_{\rm out}}\frac{e_{\rm out}}{1-e_{\rm out}^2}. \tag{7}$$

- In this limit, $K = j\cos I$.
- When $0 < \epsilon_{\rm oct}$, orbit flips become possible, and during these orbit flips, $e = e_{\rm lim}$ is attained (Lithwick & Naoz 2011; Liu et al. 2015). The range of inclinations for which this is possible is wider than the quadrupole-only case.
- Katz et al. (2011) show that, with $0 < \epsilon_{\rm oct} \ll 1$, K oscillates in a well-behaved way. An approximate analytic calculation gives an accurate prediction of this orbit-flipping window when $\epsilon_{\rm oct} \ll 1$ and when ω, the argument of pericenter of the inner orbit, is circulating. Timescale is given by Antognini (2015).

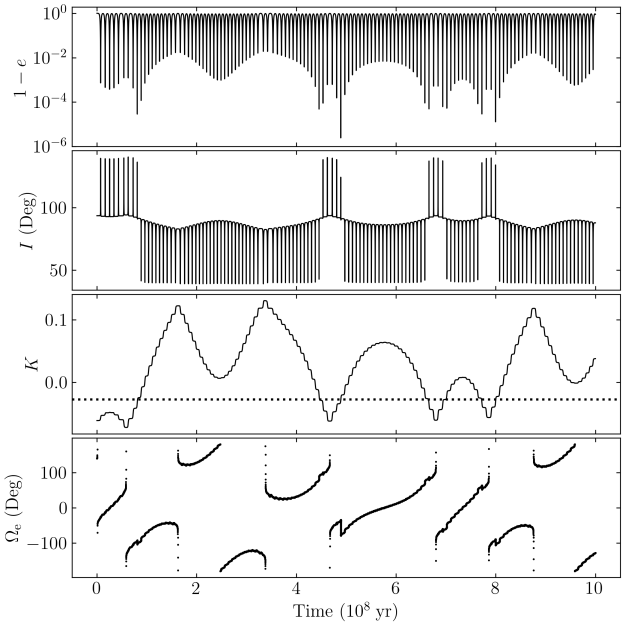

Figure 1. Fiducial simulation showing orbit flips, which occur when K crosses the dotted line $K = K_c \approx \eta/2$. $I_0 = 93.5°$. When ω is circulating, the angle Ω_e (the co-longitude of the inner eccentricity vector) changes slowly (Katz et al. 2011).

- (Muñoz et al. 2016) shows that the octupole-active region can be well fit by a fitting formula for $\epsilon_{\rm oct}$ as large as 0.07. The blue dots in top panel of Fig. 2 show that indeed the maximum eccentricity reaches $e_{\rm lim}$ within this inclination range.

2.3 Octupole-Order ZLK, General Masses

When m_1, m_2 are comparable, Eq. (7) generalizes to

$$\epsilon_{\rm oct} = \frac{m_1 - m_2}{m_{12}} \frac{a}{a_{\rm out}} \frac{e_{\rm out}}{1-e_{\rm out}^2}. \tag{8}$$

The comparable-mass regime is qualitatively different from the test-particle regime (e.g. Rodet et al, 2021). We show a fiducial simulation in Fig. 1

- No analytic solution to predict amplitude of K (generalized version) oscillations, though qualitative behavior is the same.
- Asymmetric octupole-active region (see top panels of Figs. 3–5).
- We describe the behavior with two characteristic eccentricities: $e_{\rm max}$ and an effective $e_{\rm eff}$. The latter is defined via an average over many ZLK cycles (denoted by angle brackets) and $j_{\rm eff} \equiv \sqrt{1-e_{\rm eff}^2}$:

$$\left\langle \frac{{\rm d}\ln a}{{\rm d}t} \right\rangle \approx -\frac{1}{t_{\rm GW,0}} \left\langle \frac{1 + 73e_{\rm max}^2/24 + 37e_{\rm max}^4/96}{j_{\rm min}^6} \right\rangle \equiv -\frac{421/96}{t_{\rm GW,0}} \frac{1}{j_{\rm eff}^6}. \tag{9}$$

3 WITH GW

We turn on GW, binaries will either merge or not within 10 Gyr, produces middle panels of Fig. 3.

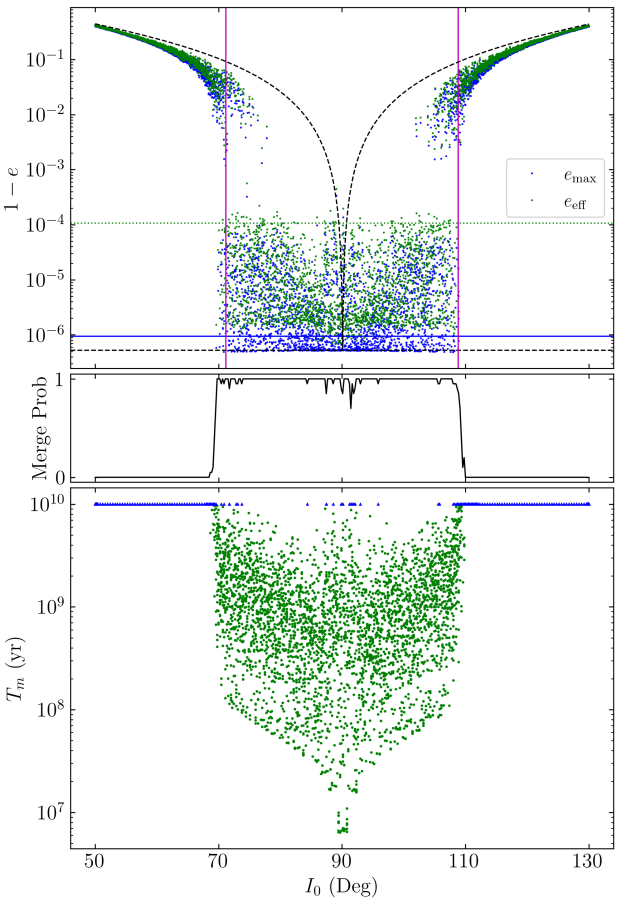

Figure 2. Fiducial parameters (a = 100 AU, $a_{\rm out,eff}$ = 3600 AU, $m_{12} = 50M_\odot$, $m_3 = 30M_\odot$) where $e_{\rm out} = 0.6$ and $q = 0.01$, i.e. in the test-particle regime $\eta \ll 1$ [Eq. (2)]. In the top panel, for each of 1000 initial inclinations, we choose 5 different random ω, $\omega_{\rm out}$, and Ω as initial conditions, then run for $500t_{\rm ZLK}$ without gravitational wave radiation. The maximum eccentricity $e_{\rm max}$ (blue dots) as well as the effective eccentricity [Eq. (9); green dots] over this period are displayed. For comparison, $e_{\rm eff,c}$ [Eq. (12)] is given by the horizontal green dashed line, $e_{\rm os}$ [Eq. (11)] is shown in the horizontal blue line, and $e_{\rm lim}$ [Eq. (6)] is shown in the horizontal blue dashed line. The vertical purple lines are the fitting formula of Muñoz et al. (2016) and accurately capture the range of initial I_0 for which $e_{\rm max}$ reaches $e_{\rm lim}$. In the bottom panel, we simulate the same initial conditions with gravitational wave radiation and record the outcome, which is either a successful merger ($T_{\rm m} < 10$ Gyr; green dots) or not ($T_{\rm m} > 10$ Gyr; blue triangles). Since each I_0 is run multiple times with random ω, $\omega_{\rm out}$, and Ω, we can estimate a merger probability for each I_0, depicted in the middle panel. In the top panel, systems are expected to merge according to the GW-free simulations if $e_{\rm max} > e_{\rm os}$ (blue dots below blue line) or if $e_{\rm eff} > e_{\rm eff,c}$ (green dots below green line). This criterion accurately captures the regions for which the dissipative simulations predict nonzero merger probabilities (middle panel).

- Define $e_{\rm os}$, and $j_{\rm os} = \sqrt{1-e_{\rm os}^2}$, the $e_{\rm max}$ required to produce a one-shot merger ZLK:

$$j\,(e_{\rm os}) \left.\frac{{\rm d}\ln a}{{\rm d}t}\right|_{e=e_{\rm os}} \sim \frac{1}{t_{\rm ZLK}}, \tag{10}$$

$$j_{\rm os}^6 = \frac{256}{5} \frac{G^3 \mu m_{12}^3}{m_3 c^5 a^4 n} \left(\frac{a_{\rm out,eff}}{a}\right)^3. \tag{11}$$

If an IC has $e_{\rm max} \gtrsim e_{\rm os}$, then gives one-shot merger. See comparison between top and middle panels for Figs. 2–5.

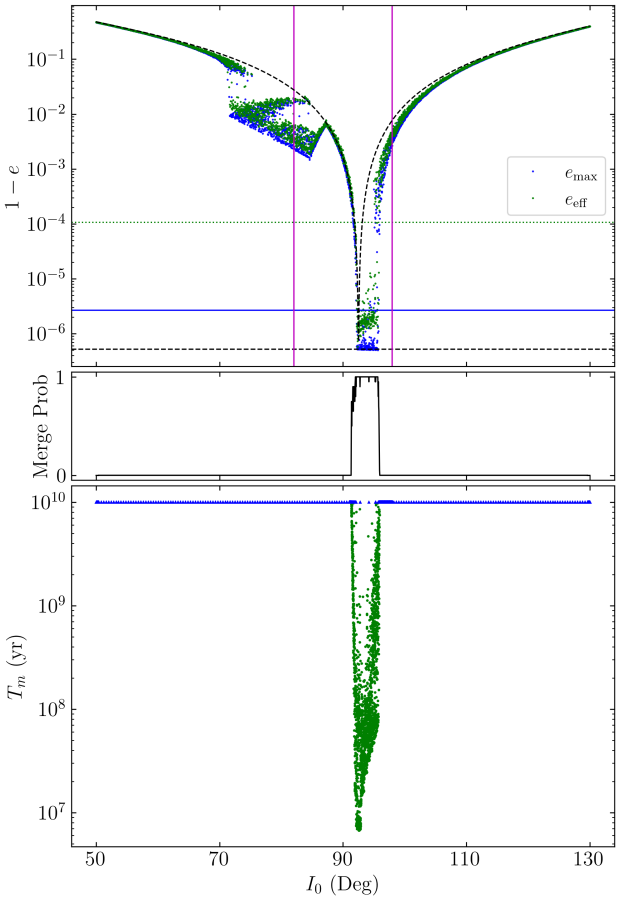

Figure 3. Same as Fig. 2 but where instead $q = 0.5$, so $\eta \approx 0.087$ is nonnegligible, and $\epsilon_{\rm oct} \approx 0.007$. The Muñoz et al. (2016) fitting formula (the vertical purple lines in the top panel) no longer accurately captures the octupole-active inclinations, and none of the panels are symmetric about $I_0 = 90°$. However, the $e_{\max}$ and $e_{\rm eff}$ criteria still accurately predict the regions where the merger probability is nonzero.

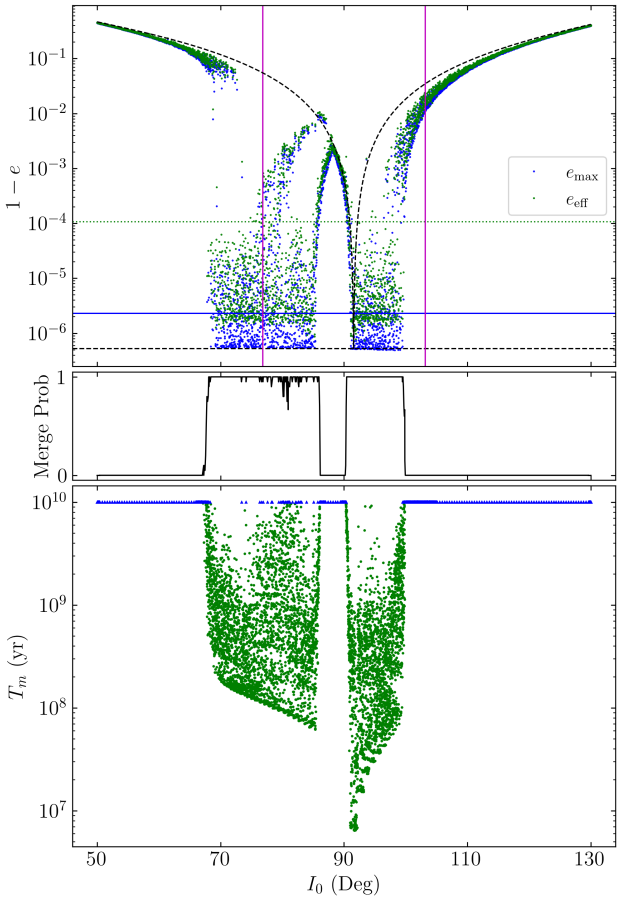

Figure 4. Same as Fig. 3 but for $q = 0.2$, $\eta \approx 0.054$, and $\epsilon_{\rm oct} \approx 0.014$. Note that prograde perturbers ($I_0 < 90°$) are able to induce mergers, unlike in Fig. 3. A "gap" in merger probabilities for $I_0 \approx 90°$ is evident, which is discussed further in Appendix A.

- Define $e_{\rm eff,c}$ and $j_{\rm eff,c} \equiv \sqrt{1-e^2_{\rm eff,c}}$, the critical effective eccentricity, such that

$$\left\langle \frac{{\rm d}\ln a}{{\rm d}t} \right\rangle = \frac{421/96}{t_{\rm GW,0} j^6_{\rm eff,c}} = 10\ {\rm Gyr}. \tag{12}$$

If an IC has $e_{\rm eff} \gtrsim e_{\rm eff,c}$, then gives gradual merger.

For wide binaries, systems generally satisfy $e_{\max} \gtrsim e_{\rm os}$ if and only if they satisfy $e_{\rm eff} \gtrsim e_{\rm eff,c}$. However, this need not be the case, see Fig. 6.

4 MASS RATIO SIGNATURE IN A POPULATION OF MERGING BBHS

A physically representative ensemble is beyond the scope of this paper, and we instead focus on simple, illustrative populations of BBH to demonstrate the effect.

4.1 Fixed Tertiary Eccentricity

We first consider the simplified case where the tertiary eccentricity is fixed, and seek the merger probability as a function of mass ratio q. For these, we let $\cos I_0$ be drawn uniformly from the range $[-1, 1]$, and fix everything else. See Fig. 7. This suggests that low mass ratio mergers should be more common.

- For sufficiently small $\epsilon_{\rm oct}$, the merger probability does not depend on $e_{\rm out}$ and q separately but only on their combination via $\epsilon_{\rm oct}$.
- However, when $\epsilon_{\rm oct}$ is sufficiently large, an $e_{\rm out}$ dependence is introduced. This is because the size of the gap (see e.g. Fig. 5), and the value of $\epsilon_{\rm oct}$ when prograde systems are able to merge, depend on q through η. A discussion of this gap is in Appendix A.

We also examine what happens when $a = 50$ AU; This figure is still being generated.

4.2 Distribution of Tertiary Eccentricities

We can also draw $e_{\rm out} \in [0, 0.9]$. We try either uniform probability or thermal $P(e_{\rm out}) \propto e_{\rm out}$. The results are given for our fiducial $a_{\rm out,eff} = 3600$ AU in Fig. 8. For comparison, we also show the results when $a_{\rm out,eff} = 5500$ AU.

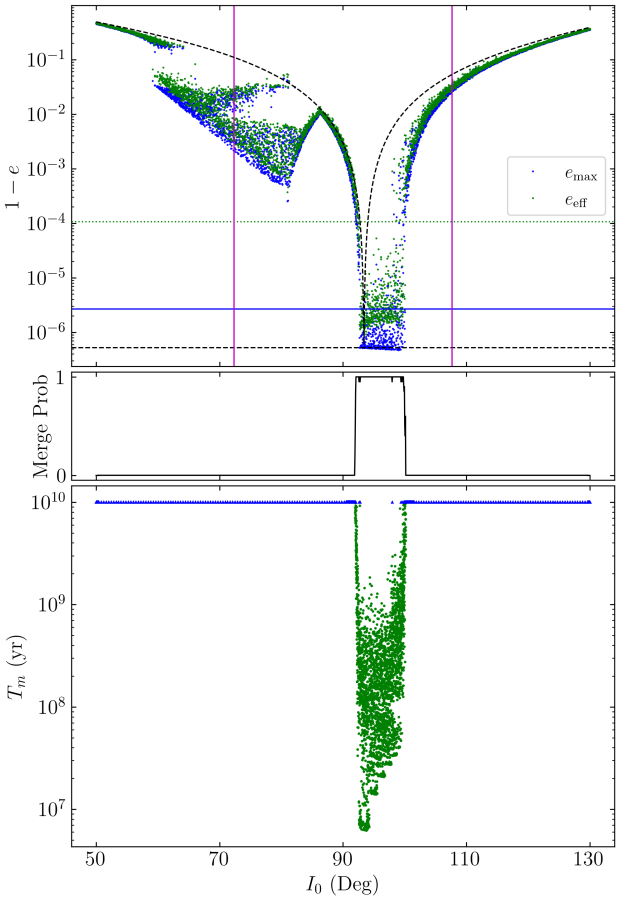

Figure 5. Same as Fig. 3 but $e_{\rm out} = 0.9$ while holding $a_{\rm out,eff} = 3600$ AU constant. Here, $\eta \approx 0.12$ while $\epsilon_{\rm oct} \approx 0.019$. Note that even though $\epsilon_{\rm oct}$ is larger here than in Fig. 4, no mergers are possible here with a prograde perturber. This is because η is more than twice as large for these parameters.

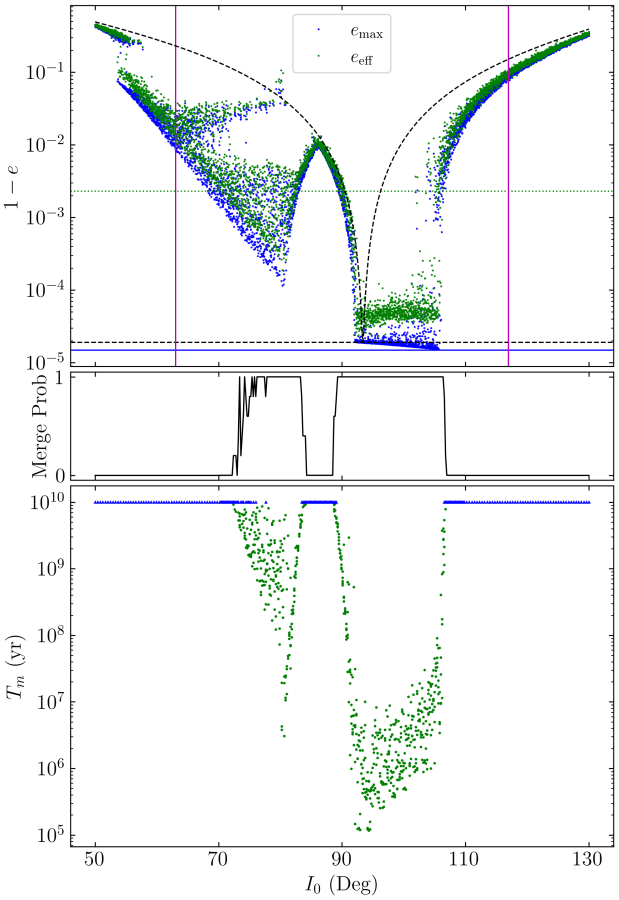

Figure 6. Same as Figs. 2–4 but for a compact inner binary; the parameters are $a = 10$ AU, $a_{\rm out,eff} = 700$ AU, $m_{12} = 50M_\odot$, $m_3 = 30M_\odot$, and $e_{\rm out} = 0.9$, $q = 0.4$. Note that when the perturber is prograde ($I_0 < 90°$), $e_{\max} < e_{\rm os}$ but $e_{\rm eff} > e_{\rm eff,c}$, which predicts that systems are able to merge. This prediction is borne out by simulations with GW radiation (middle and bottom panels).

- Note: LIGO-band eccentricities are small, but nonetheless show a small q dependence, which may be detectable in the LISA band.

4.3 Effect of Smaller Mass Ratios

Intuitively, $q \to 0$ means $t_{\rm GW,0} \to \infty$ and no mergers. This would predict more large-mass-ratio mergers, opposite to our observed trend. Why is this?

When orbital flips occur, $e_{\max}$ attains $e_{\rm lim}$. This induces one-shot mergers when $e_{\rm lim} > e_{\rm os}$, or when

$$\left(\frac{a}{a_{\rm out,eff}}\right) \gtrsim 0.0118 \left(\frac{a_{\rm out,eff}}{3600\ {\rm AU}}\right)^{-7/37} \left(\frac{m_{12}}{50M_\odot}\right)^{17/37} \times \left(\frac{30M_\odot}{m_3}\right)^{10/37} \left(\frac{q/(1+q)^2}{1/4}\right)^{-2/37}. \quad (13)$$

This shows that q must be changed by many orders of magnitude to transition between a parameter regime where one-shot mergers occur at orbital flips to one where such mergers fail to occur.

5 CONCLUSION

- Primordial q distribution in massive stellar binaries: tends to be skewed towards smaller q to varying degrees (Sana et al. 2012; El-Badry et al. 2019).
- Eccentricity distribution of tertiary? Likely to be between uniform and thermal.
- LIGO O3a bounds on the BBH q distribution: if $P(q) = q^{\beta_q}$, then $\beta_q > 0$ at 89% or more, depending on the model (Abbott et al. 2020), implying favoring equal-mass binaries.
- Our parameters are not particularly fine-tuned. If the inner binary is tighter or the perturber farther, then the MLL16 fits are better and give the same qualitative result. If the inner binary is looser, flybys become important. If the perturber is closer, then DA breaks down.

However, if $e_{\rm lim} < e_{\rm os}$ [i.e. Eq. (13) is violated], the size of the effect can be much weaker, as most octupole-active systems no longer successfully merge within 10 Gyr unless they are near the quadrupole merger window. This implies the merger window only widens slightly even if $\epsilon_{\rm oct}$ is appreciable. Note that this does not change the trend of the effect, only its magnitude.

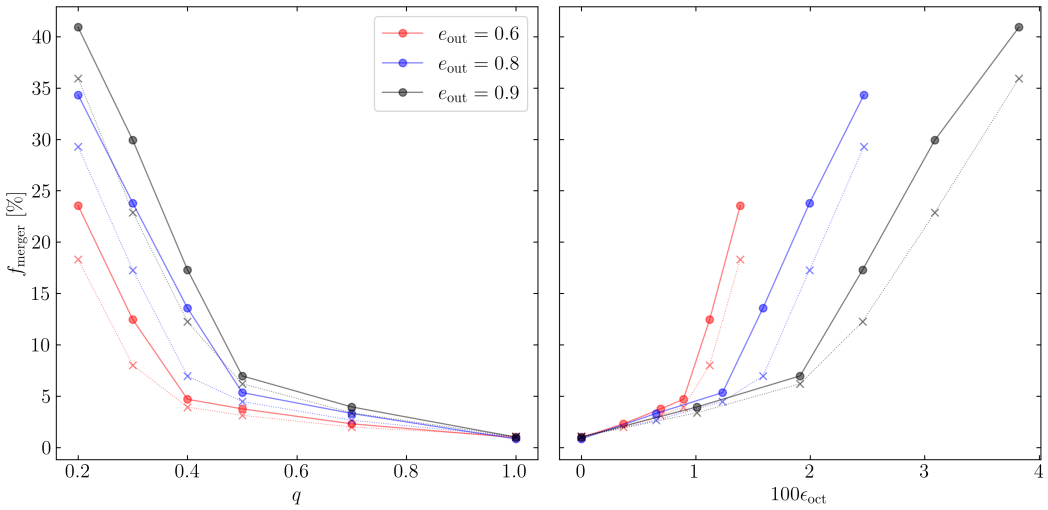

Figure 7. From Figs. 3–5, we can compute the total merger probability in the presence of GW radiation assuming $\cos I_0$ is uniformly distributed $\in [-1, 1]$. We do this for three values of $e_{\rm out}$ and six values of q and show the results with solid dots. The X's show the results when GW-free simulations are instead used to predict the total merger probability, i.e. using the criteria shown in the top panels of Figs. 3–5; good agreement is observed.

6 ACKNOWLEDGEMENTS

YS is supported by the NASA FINESST grant 19-ASTRO19-0041.

REFERENCES

Abbott R., et al., 2020, arXiv preprint arXiv:2010.14533
Anderson K. R., Storch N. I., Lai D., 2016, Monthly Notices of the Royal Astronomical Society, 456, 3671
Antognini J. M., 2015, Monthly Notices of the Royal Astronomical Society, 452, 3610
El-Badry K., Rix H.-W., Tian H., Duchêne G., Moe M., 2019, Monthly Notices of the Royal Astronomical Society, 489, 5822
Katz B., Dong S., Malhotra R., 2011, Physical Review Letters, 107, 181101
Lithwick Y., Naoz S., 2011, The Astrophysical Journal, 742, 94
Liu B., Muñoz D. J., Lai D., 2015, Monthly Notices of the Royal Astronomical Society, 447, 747
Muñoz D. J., Lai D., Liu B., 2016, Monthly Notices of the Royal Astronomical Society, 460, 1086
Peters P. C., 1964, Physical Review, 136, B1224
Sana H., et al., 2012, Science, 337, 444
Silsbee K., Tremaine S., 2017, The Astrophysical Journal, 836, 39

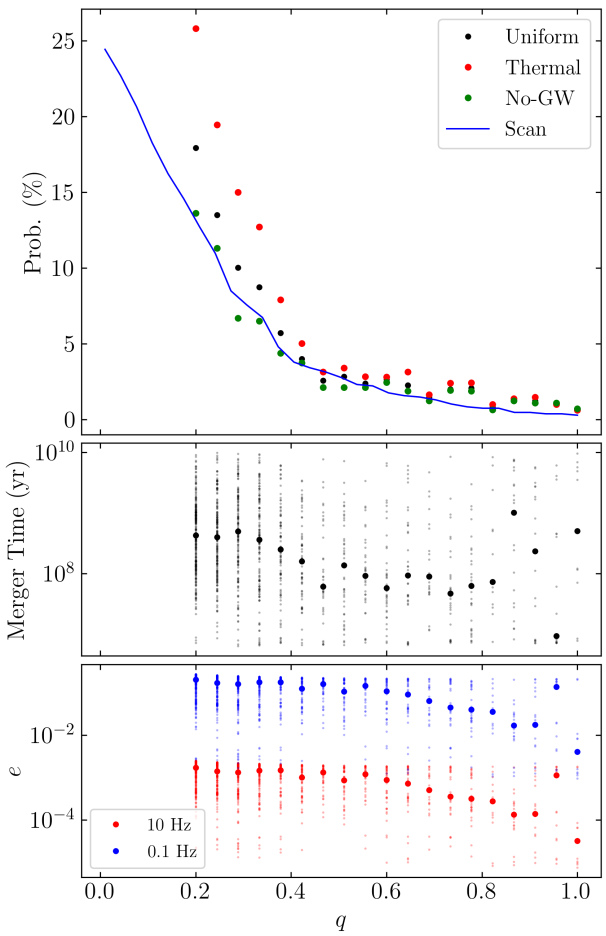

Figure 8. Merger fractions with the fiducial parameters obtained by randomly drawing $\cos I_0$ uniformly distributed $\in [-1, 1]$ and drawing $e_{\rm out}$ from either a uniform distribution ($e_{\rm out} \in [0, 0.9]$) or a thermal distribution ($P(e_{\rm out}) \propto e_{\rm out}$, $e_{\rm out} \in [0, 0.9]$). In the top panel, we show the resulting merger probabilities for a uniform $e_{\rm out}$ distribution (black) and a thermal one (red). Green dots use the same initial conditions but use the GW-free merger criteria. The blue line instead samples a dense, uniform grid in $\cos I_0$ and $q \in [0.01, 1]$ using the GW-free simulations, confirming that the non-monotonicity of the other dots is due to the random sampling of $\cos I_0$. The middle panel shows the merger time for successful mergers (the median is denoted with the large black dot). The bottom panel shows the binary eccentricity in the LISA band (0.1 Hz) and in the LIGO band (10 Hz).

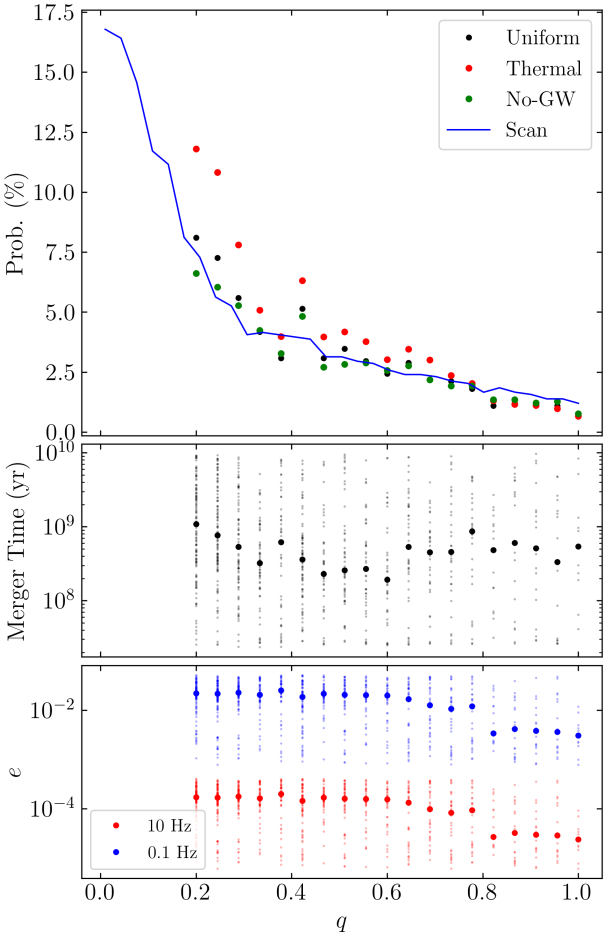

Figure 9. Same as Fig. 8 but for $a_{\rm out,eff} = 5500$ AU.

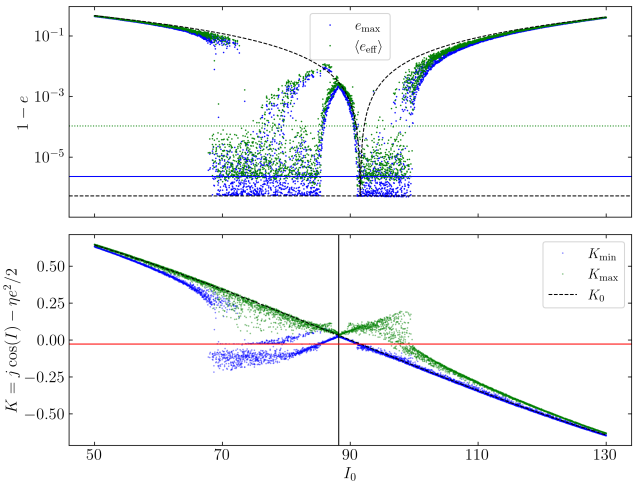

Figure A1. Top panel is the same as the top panel of Fig. 4. The bottom panel shows the range of oscillation in K, denoted by $K_{\rm min}$ and $K_{\rm max}$, for the same parameters. The critical $K = \eta/2$ for orbit flipping is shown with the horizontal red line. It can be seen that when $K_{\rm min} < \eta/2 < K_{\rm max}$ that $e_{\rm max} \simeq e_{\rm lim}$ in the top panel. It is therefore clear that the gap in $e_{\rm max}$ excitation is due to a limited range of oscillation in K.

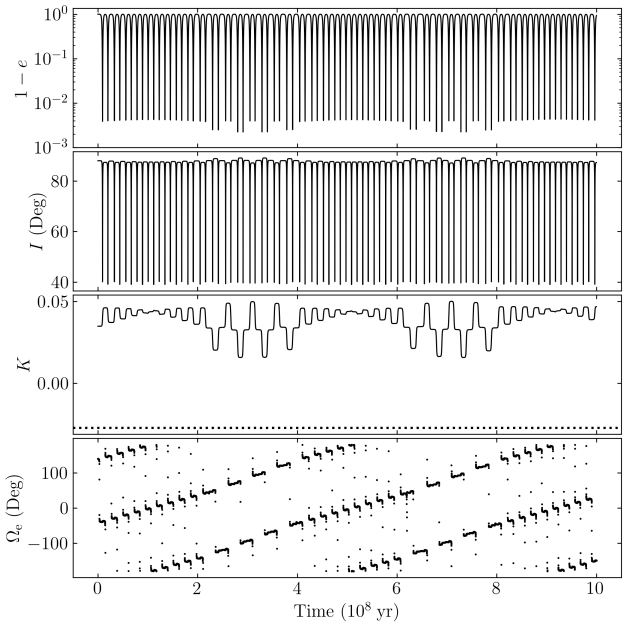

Figure A2. Example simulation where $\Omega_{\rm e}$ is primarily circulating, which suppresses the amplitude of oscillation of K. As a result, the orbit does not flip.

APPENDIX A: ORIGIN OF OCTUPOLE-INACTIVE GAP

- Show the $K_{\rm min}$ and $K_{\rm max}$ plot, Fig. A1.
- Is because librating! example simulation where librating, Fig. A2.
- Point out that the character of the circulation-libration transition changes when $\epsilon_{\rm oct}$ is substantial, to not only depend on ω, Fig. A3.

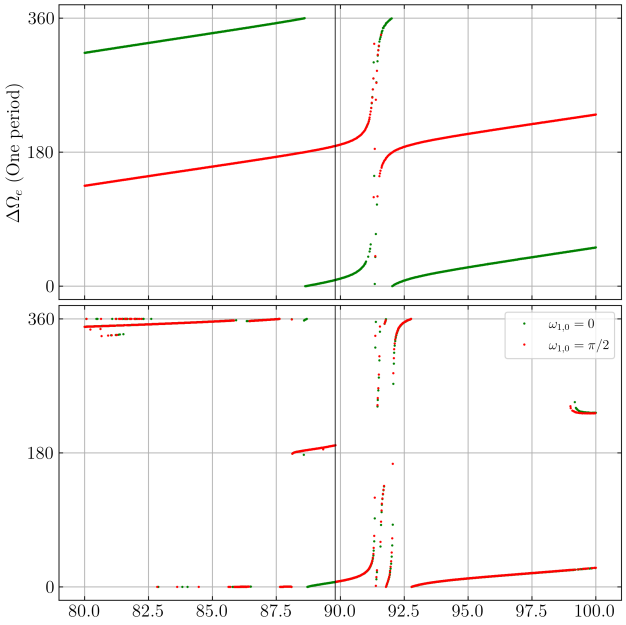

Figure A3. Plot of $\Delta\Omega_e$, the change in the co-longitude of the inner eccentricity vector Ω_e over a ZLK cycle, for different initial conditions and when octupole terms are off/on. In the top panel, the octupole terms are neglected, and $\omega_0 = 0$ results in circulation ($\Delta\omega = 0$ and $\Delta\Omega_e = 180°$) while $\omega_0 = \pi/2$ results in libration, as expected. In the bottom panel, the octupole terms are included, and it is seen that the circulation-libration transition no longer depends on ω_0 but instead on I_0.